SPC Journal of Environmental Sciences, 8 (1) (2026) 36-45

SPC Journal of Environmental Sciences

Website: www.sciencepubco.com/index.php/JES
https://doi.org/10.14419/34936g02
Research paper

Kinetic and Mechanistic Analysis of Methylene Blue Adsorption by Manganese-Based Metal-Organic Framework for Dye wastewater Remediation

Emokensi Danjuma Ika [1], Emmanuel Ba'aku AttahDaniel [2] *, Andebutop Sule [3], Emem Ikpeme Bassey [4], Musa Samuel [2], Judean Jude Rabo [2], Sarah Amayindi AtttahDaniel [2]

[1] Department of Industrial Chemistry, Federal University Wukari, PMB 1020, Katsina-Ala Road Wukari Taraba State, Nigeria
[2] Department of Chemistry, Federal University Wukari, PMB 1020, Katsina-Ala Road Wukari Taraba State, Nigeria
[3] Key Laboratory of Geographical Processes and Ecological Security in Changbai Mountains, Ministry of Education, School of Geographical Sciences, Northeast Normal University, Changchun, China.
[4] Analytical Chemistry Research Group, Department of Pure and Applied Chemistry, University of Calabar, PMB 1115 Calabar, Cross River State, Nigeria
**Corresponding author E-mail: attahdaniel@fuwukari.edu.ng*

Abstract

Water pollution, particularly from dye effluents, poses a significant threat to water quality and human health. This study investigated the methylene blue (MB) adsorption potential of a manganese-benzene 1,4-dicarboxylic acid organic framework (Mn-MOF), synthesized using reflux controlled solvothermal method. The Mn-MOF was characterized by scanning electron microscopy (SEM), Energy dispersive X-ray spectroscopy (EDX), Fourier-transform infrared spectroscopy (FTIR), and pH-point of zero charge (pHpzc) analysis. Batch adsorption experiments were conducted to evaluate the adsorption capacity of Mn-MOF, with a focus on the effects of contact time. Kinetic studies, including the pseudo-first-order (PFO), pseudo-second-order (PSO), fractal pseudo-second-order (FPSO), and Webber-Morris intra-particle diffusion (IPD) models, were employed to assess the adsorption mechanism and equilibrium behavior. The results indicated that the PSO model best described the MB adsorption process, with the FPSO model showing an r^2 value of 0.941. The low C value of 0.16 mg/g suggested minimal contribution from intra-particle diffusion to the adsorption process. Given the promising results, this study highlights the potential of Mn-MOF for dye wastewater remediation.

Keywords: *Adsorption Kinetics; Dye Removal; Methylene Blue; Manganese Metal-organic Framework (Mn-MOF); Remediation; Wastewater.*

1. Introduction

Water is a vital essential natural resource for human survival and development [1]. However, global industrial advancement has continuously impacted both the quantity and quality of water resources over the years [2]. The drive to enhance human comfort and progress has led to the introduction of pollutants into the environment, particularly through industrialization. Waste products from industrial processes include heavy metals, polycyclic hydrocarbons, and dyes. Industries producing textiles, cosmetics, paper, leather, and food predominantly discharge dyes into water bodies, rendering these water sources unsuitable for human, recreational, and industrial use [3].
Reports by Akter et al indicated that approximately 2.8 x 10^5 tons of textile dyes are released into water bodies annually [4]. This has severe implications for water quality, with the most pressing issue being the global shortage of clean water. Dyes, which are colored organic compounds, are also carcinogenic [5]. The temperature of dye effluent, typically between 65 and 75°C, creates a heat reservoir that disrupts the thermal balance of surrounding water bodies near textile factories [6]. According to the UN, an estimated 5 to 10 million people die annually from diseases related to drinking contaminated water [7]. Effective treatment of polluted wastewater is critical, as approximately 10-15% of dye is naturally lost during the dyeing process and is released with the effluent [8]. The chemical structure of dye wastewater contains aromatic amines (Ar-NH_2), naphthyl ($C_{10}H_{17}CH_2$), and azo (-N=N-) groups, making treatment challenging. These compounds are carcinogenic to aquatic fauna and mutagenic to aquatic flora.
To treat organic dye wastewater, various methods, including coagulation, membrane filtration, adsorption, photo-catalysis, and advanced oxidation, have been developed [9]. Among these methods, adsorption is considered one of the most effective in terms of design, operation, setup, capacity, ease of regeneration, and cost. It produces no toxic or harmful pollutants, incurs low capital and operational costs, generates no sludge, and results in high-quality treated water [10].

Copyright © Emokensi Danjuma Ika et al. This is an open access article distributed under the Creative Commons Attribution License, which permits unrestricted use, distribution, and reproduction in any medium, provided the original work is properly cited.

Despite being eco-environmentally friendly, adsorption techniques often fall short in eliminating contaminants, raising concerns about the lingering presence of aqueous pollutants [11]. Adsorbents such as activated carbon, zeolites, and polymeric materials have been commonly used to remove organic dye pollutants [12]. However, activated carbon has limitations, including non-selectivity, inefficiency against dispersed and vat dyes, and high cost [13]. These materials generally have low void space and adsorption capacity. However, new adsorbents, like metal-organic frameworks (MOFs) and hybrid composites, offer promising properties such as high specific surface area, large pore volume, and tunable pore sizes, which can regulate adsorption capacity [14]. MOFs, a class of porous materials, contain a bridging ligand (organic linker) connected to a secondary building unit (transition metal ion) via coordination bonds [15]. These coordination bonds enable efficient crystallization, mild synthesis conditions, versatile design, and various metal compositions. The large surface area (up to BET 6000 m^2/g) and large pore size (up to 5 nm, with approximately 90% of the volume) make MOFs highly effective. Due to their organic functionality and high thermal and mechanical stability, MOFs are promising materials for various applications.
Metal organic frameworks (MOFs) have garnered significant attention due to their fascinating architecture, topologies, and increasing range of potential applications, including functional materials, magnetism, luminescence, catalysis, gas separation, storage, and drug delivery [16]. Recent studies by Zhao et al revealed that charged MOFs can remove dyes through guest molecule substitution [17], adsorb hydrogen (H_2), and capture carbon dioxide. MOFs have also been identified as effective adsorbents for removing methylene blue (MB) from wastewater [18]. Furthermore, MOFs and their composites with polyvinyl alcohol (PVA/MOF) have shown excellent adsorption properties for removing Lead (II) ions from aqueous solutions [19]. Other works, such as Cu-MOF prepared using the ultrasound irradiation method, demonstrated an excellent adsorption capacity for methylene blue [35]. Cu@Co-MOFs prepared via a one-step hydrothermal method also demonstrated strong adsorption capacity for the removal of methylene blue [34]. Also, UiO-66 MOF, with a high hydrothermal stability among MOFs synthesized via microwave method, showed a very attractive characteristic as an adsorbent to toxic chemicals from wastewater [31]. A bimetallic-UiO-66 MOF used to adsorb cationic dyes showed a maximum adsorption capacity of 14.84mg/g for MB, while MnO_2/IRMOF-3 nano-composite synthesized by a "bottle-around-ship" method showed very promising potential in the adsorption of MB from aqueous solution with a maximum adsorption capacity of 11mg/g. In this work, a manganese-based MOF was synthesized via a reflux-controlled solvo-thermal method [20], and its methylene blue adsorption characteristics were studied.

2. Materials and Methods

2.1. Chemicals

The chemicals used were supplied by Acros Organics (Belgium), Promark Chemicals (India), Merck and Emsure (Germany), and Labochem (Greece).

2.2. Experimental procedures

The procedure used for the synthesis of Mn-MOFs is described below.

2.2.1. Manganese-metal organic framework (Mn-MOF)

Mn $(NO_3)_2.4H_2O$ (0.0159 mol) and $C_8H_6O_4$ (0.0159 mol) were dissolved in 80 mL of H.CO. N (CH_3) with mild stirring. The reflux system was sealed and refluxed for 8 h at 100 ℃. The crystals formed from the reaction were collected by centrifugation and washed with methanol at least three times, dried in an oven at 75 ℃ for 45 min, and labelled as Mn-MOF and preserved for further use.

2.3. Characterization

A Zeiss Auriga Field Emission Scanning Electron Microscope, coupled with an Energy Dispersive X-ray (EDX) equipped with an Oxford X-max detector with Aztec software, was used to determine the surface morphology and the elemental composition of Mn-MOF, respectively. The porosity of the material was determined via the Brunauer, Emmett, and Teller (BET) analysis. While the oxygen-metal bond (O-Mn) in Mn-MOF and the functional groups present were studied with the aid of a Thermo Scientific, NICOLET iS50 Fourier Transform Infra-red spectrophotometer by scanning the crystals over the spectral region of 500 to 4000 cm^{-1}. The point of zero charge (pHpzc) of the material was determined with the help of an XS Instruments pH meter used in obtaining the pH and measurement of the zeta potentials. The residual concentration of the batch adsorption process was determined by a T80+ UV/Visible spectrometer.

2.3.1. Determination of point of zero charge (pHpzc)

The determination of the point of zero charge (pHpzc) of the adsorbent is described as follows. 20 cm^3 of 0.01M NaCl solution was placed in various polyethylene bottles. The pH values were adjusted to between 4 and 10 by adding 0.1M HNO_3 or 0.1M NaOH to each of the solutions. About 20 mg of the adsorbent Mn-MOF was added to each vial and shaken for 1 h on a shaker at 200 rpm to mix properly, and allowed to stand for 48 h. The pH values of the solution with their corresponding zeta potential were recorded. A curve of the pH measured after 48 h against the zeta potential was plotted. The (pHpzc) is the point where the curve intercepts the pH axis of the plot.

2.3.2. Adsorption kinetic studies

Adsorption kinetics studies of Mn-MOF were performed by varying the contact time between the adsorbent and the adsorbate (MB). The experiment was carried out in duplicate for reproducibility, and the average values obtained were recorded. These were carried out for periods ranging from 5, 10, 15, 30, 60, 120, 180, 240, and 360 min, respectively. In each reaction vessel (polyethylene tube), about 20 mg of Mn-MOF and 10 mL of MB solution (50 ppm) were mixed and labelled appropriately with the respective time variations specified above at room temperature (24 ℃). The mixture was then agitated in a shaker at 200 rpm until each required time is reached and the appropriate reaction vessel was withdrawn, centrifuged at 4000 rpm, and the supernatant was used to determine the amount of MB left in solution.

2.4. Data analysis

2.4.1. Adsorption kinetics model

The quantity (mg/g) of MB uptake by Mn-MOF was estimated using the equation

$$q_e = \frac{v}{m}(C_o - C_e) \quad (1)$$

Where the initial concentration of MB = C_o, final concentration of MB = Ce, the amounts of MB adsorbed in mg/g at equilibrium = q_e, v and m are the volume of the solution (mL) and mass (g) of adsorbent used, respectively.
To understand the kinetics of the adsorption process, various kinetic models were deployed to study the process, which enhanced the understanding of the mechanism involved in the process. Some of the widely used kinetic models engaged in this study are discussed below with their mathematical expressions.

2.4.2. Pseudo-first-order model

The pseudo-first order model (PFOM) rate equation is widely used to study the kinetics of sorption processes. It was proposed by Lagergren in 1898. The linearized equation is expressed as:

$$\frac{dq}{dt} = k_f(q_e - q) \quad (2)$$

Here, q_e (mg/g) is the adsorption capacity at equilibrium, while q (mg/g) is the adsorption capacity at time t, and the rate constant is k_f (/min). When the boundaries q = 0 at t = 0 and q = q_e At t = t is introduced and equation 2 is integrated, the equation becomes as shown below.

$$\log(q_{e-}q) = \log q_e - \frac{k_f t}{2.303} \quad (3)$$

The computation of the adsorption rate constant, k_f, can be deduced from the linear plot of $\log(q_{e-}q)$ versus t. The nonlinear version of equation 3 is represented in equation 4

$$q_e = q_t\left(1 - e^{-k_1 t}\right) \quad (4)$$

2.4.3. Pseudo-second-order model

The pseudo-second order model (PSOM) is considered very applicable to chemisorption processes. Equation 5 gives the mathematical expression of the pseudo-second order model [21].

$$\frac{d_q}{d_t} = k_s(q_e - q)^2 \quad (5)$$

Where q_e (mg/g) is the adsorption capacity at equilibrium, q (mg/) is the adsorption capacity at time t. Equation 5 on the introduction of, q = 0 at t = 0 and q = q_e at t = t, as boundary conditions and integrated becomes.

$$\frac{t}{q} = \frac{1}{k_s {q_e}^2} + \frac{t}{q_e} \quad (6)$$

From the linear plot of t/q against t, the values of q_e and k_s can be calculated. If t tends to zero, the expression becomes:

$$h = k_s {q_e}^2 \quad (7)$$

Where the initial adsorption rate (mg/g) = h
The non-linear version of the PSOM is given in equation 8.

$$q_e = \frac{k_2 q_e^2 t}{1 + k_2 q_e t} \quad (8)$$

Where, q_e is the quantity of MB adsorbed (mg/g) at equilibrium and k_2(g/mg/min) is the rate constant of PSOM.

2.4.4. The homogeneous Fractal Pseudo-Second Order Model (FPSOM)

The FPSOM is yet another model used in modelling the batch adsorption data. Equation 9 shows the mathematical expression of the FPSOM model.

$$q_{t=} \frac{k_f q_e^2 t^\alpha}{1 + k_f q_e t^\alpha} \quad (9)$$

Where the amount of pollutant adsorbed at equilibrium and time t are given by,q_e and q_t all in (mg/g), the fractional time index is given by α, and the rate constant is given by k_f (g/mg/min).

2.4.5. Intra-particle diffusion model

The Webber and Morris (1963 intra-particle diffusion (IPD) kinetic models are given in equation 10.

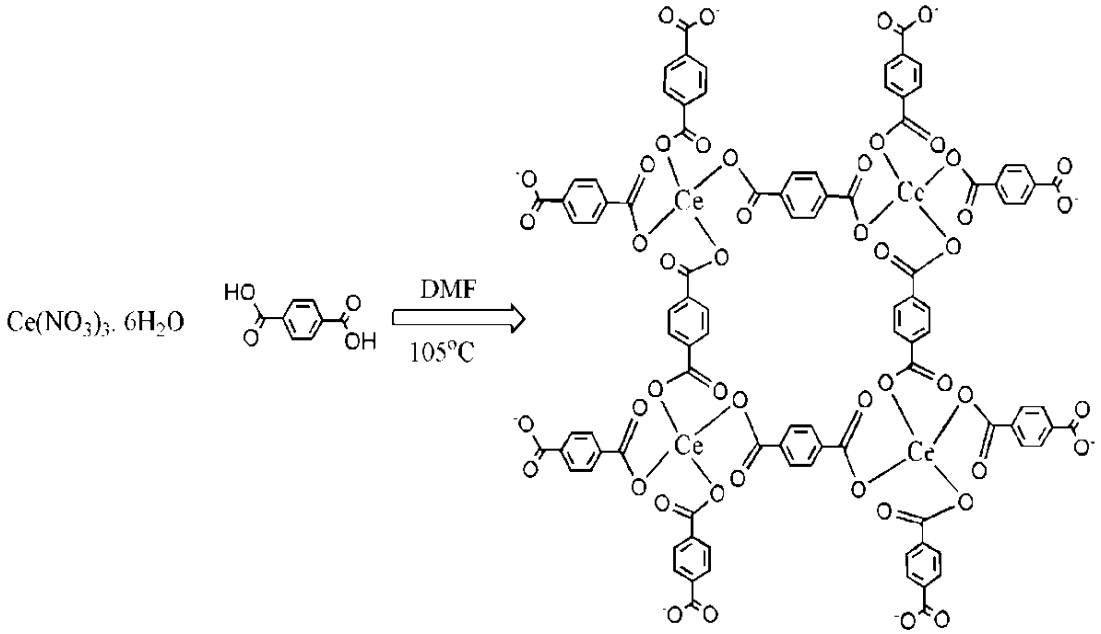
$$q_t = k_i(t^{1/2}) + C \quad (10)$$

Where q_t is the quantity of MB adsorbed in (mg/g) at time t, ki (g/gmin$^{1/2}$) is the rate parameter of IPD control stage, and C is the surface concentration. A plot of q_t versus $t^{1/2}$ should give a straight line with the slope equal to K_i. The larger the value of C, the greater is the contribution of the surface sorption in the rate-determining step. Also, the application of the intra-particle diffusion mechanism in a sorption process is determined by (i) a high correlation coefficient (r^2) value. (ii) the straight line of q_t vs. $t^{1/2}$ passing through the origin for the plot (C = 0), intra-particle diffusion is the rate-limiting step. (iii) If Ci (intercept) < 0, it suggests that more than one process determined the mechanism of the sorption process.

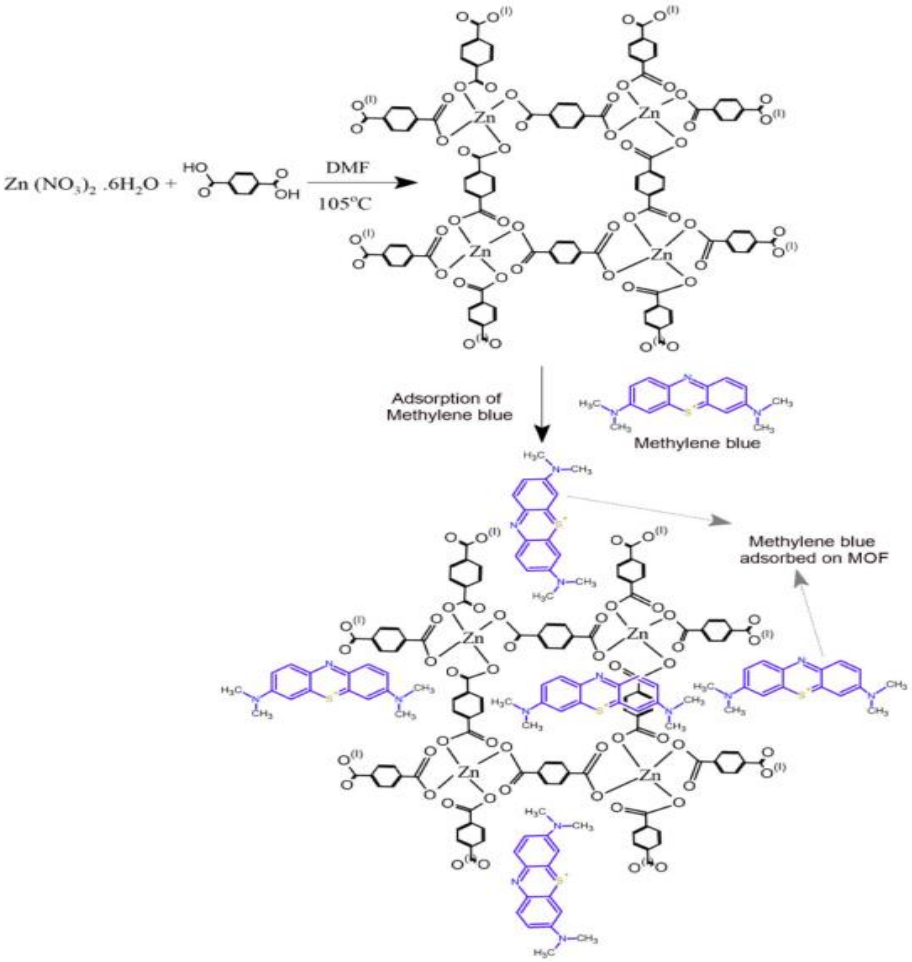
The experimental data obtained from the kinetic study were fitted into the pseudo first order (PFO), pseudo-second order (PSO), and the homogeneous fractal pseudo-second order (FPSO) discussed above, and the Webber-Morris intraparticle diffusion kinetic (IPD) model to evaluate the adsorption mechanism of MB onto the Mn-MOF. The models' fittings and parameters were further generated using Origin Pro 2015 software.

3. Results and Discussion

The synthesis factors, such as the solvent system, organic ligands, nature of metal ions, molecular interactions, couterions as well as hydrogen bonding and π-π interactions, which influence the self-assembling process in the preparation of metal-organic frameworks, play a vital role in determining the nature of the structure of the frameworks of the final product [22]. The ligand in this study is 1, 4 Benzene dicarboxylic acid (1, 4 BDC), while the metal ions are Mn^{2+}. In the synthesis process, coordination bonds are usually formed via deprotonation between the metal ions and the carboxylic group of the ligand in a solvent system to form an extended polymeric structure, as shown in Scheme 1, while Scheme 2 illustrates the form that adsorption of methylene blue will conform to. In this study, Mn-MOF was characterized using FTIR, SEM /EDX, and the pH point of zero charge (pHpzc)



Scheme. 1: Polymeric Structure Synthesized Mn-MOF Is Expected to Conform to Drawn Using ChemDraw Software.



Scheme 2: Scheme for Mn-MOF Adsorption of Methylene Blue [23].

2.5. Fourier transform infra-red spectroscopy (FTIR)

FTIR analysis confirmed the successful coordination between manganese ions and carboxylate groups of the organic linker. The linker, 1, 4 BDC, and Mn-MOF synthesized were characterized using FTIR. The spectra are presented in Fig.1. The linker 1, 4 BDC showed −OH stretching vibration mode's broad peak at 3200 cm−1, and in Mn-MOF, it remained broad.

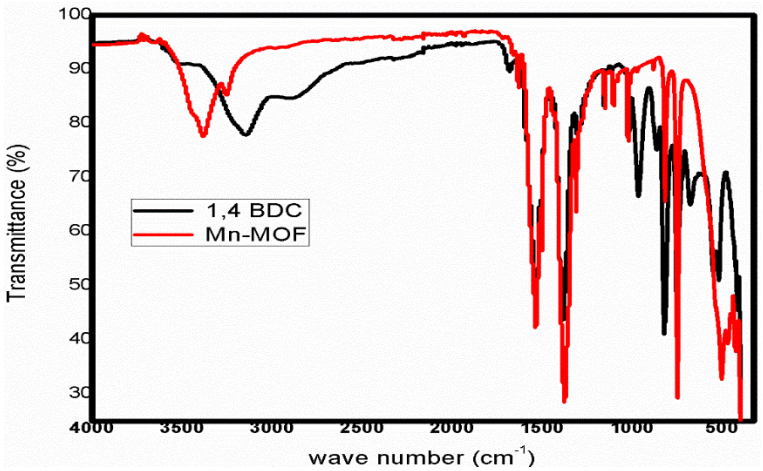


Fig. 1: FTIR Spectra of 1,4 BDC and Mn-MOF.

The peaks observed in 1572, 1508, and 1421 cm^{-1} in the spectra were assigned to the vibration modes of the –C=O of the carboxylic group from the 1, 4 BDC and the carboxylate groups of Mn-MOF.
The C−H bending vibration mode peaks of the 1, 4 BDC linker and Mn-MOF were observed at 1277 cm^{-1}. While the peaks at 1103.8 cm^{-1} for Mn-MOF were assigned to C−N stretching vibration modes from DMF. Previous studies supported the assertion that a small quantity of DMF molecules was retained on the surface of Mn-MOF [23]. The sharp peak at 744.9 cm^{-1} for the Mn-MOF spectrum is ascribed to benzene ring C-H bending vibration. While the peak at 504.5 cm^{-1} in the Mn-MOF spectrum was attributed to the Mn-O bending vibration

2.6. Scanning electron microscopy and energy dispersive X-ray spectroscopy

SEM analysis revealed an irregular and homogeneous laminar structure that is closely stacked in morphology (F.2 (a and b).

2.7. Energy dispersive X-ray spectroscopy (EDX)

Energy dispersive spectroscopy spectrum of Mn-MOF is presented in Fig.3, while Table 1 presents the percentages of the elements C, Mn, O, as, 35.79%, 49.01% and 14.46%, respectively. This confirmed the elemental content of the Mn-MOF prepared.

2.8. Point of zero charge (pHpzc) determination

The point of zero charge (pHpzc) values of the Mn-MOF was evaluated between pH 2 and 12; the results plotted are shown in Fig. 3, and revealed the point of zero charge (pHpzc) value of Mn-MOF as 7.0. This implied that the surface of Mn-MOF would carry enough positive charges (electron accepting) at the pH 2 to pH 6.9 and negative charges within the alkaline region (pH 7.1 to pH 12) and hence would be electron donating [24].

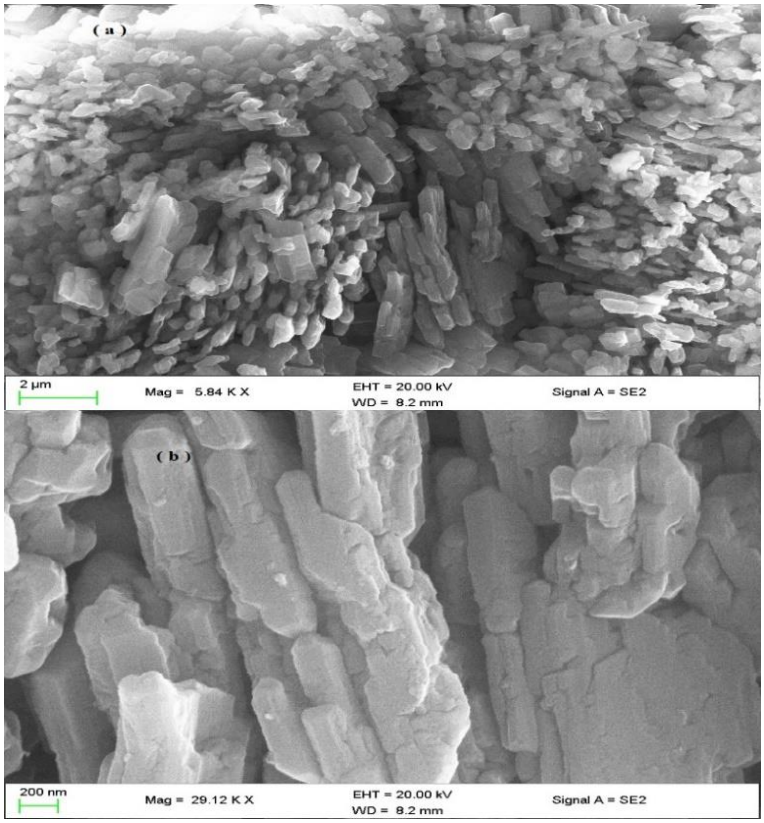


Fig. 2: SEM Images of Mn-MOF.

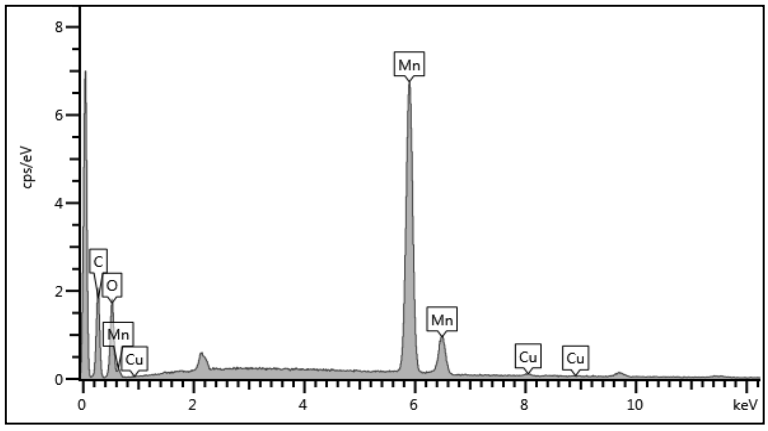


Fig. 3: EDX of Mn-MOF.

Table 1: Percentage Composition of the Elements That Make Up Mn-MOF

Elemental content	Wt%	Wt% Sigma
C	35.79	0.35
O	14.46	0.22
Mn	49.01	0.31
Cu	0.74	0.10
Total	100.0	

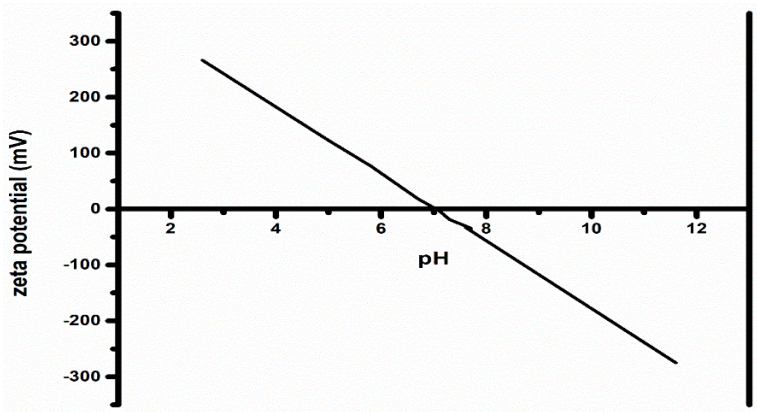


Fig. 3: Plots of Zeta Potential (Mv) Versus pH Showing the Point of Zero Charge (pHpzc) of Mn-MOF.

2.9. Adsorption studies

2.9.1. Effect of time on adsorption kinetics

The effect of time is one of the most important parameters used to determine the efficiency of an adsorbent in the removal of an adsorbate from aqueous solution. The need to minimize the holding time of industrial wastewater in treatment plants requires that maximum sorption takes place within the minimum possible time [25]. In the study of the kinetics for the adsorption of methylene blue by Mn-MOF, the rate of removal was fast and reached equilibrium within 180 min (Fig. 4).

The experimental data from the effect of time for Mn-MOF were fitted into four kinetic models: the pseudo-first order (PFO), pseudo-second order (PSO), fractal pseudo-second order (FPSO), and Webber-Morris intra-particle diffusion model (IPD) to enable the prediction of the possible mechanisms that governed the uptake of methylene blue (MB) by Mn-MOF, as shown in Fig. 5 (a-d). While the values for each of the parameters in the respective models are shown in Table 2. Considering the correlation coefficient (r^2), (0.950) value for Mn-MOF, the PSO model best fits and describes the adsorption process for Mn-MOF. However, the FPSO model had an r^2 value of 0.941, which is also very close to unity, with a QE of 2.80 mg/g removal of MB, which is a better performance in the removal of MB compared to the 2.37 Mg/g obtained for the PSO model. The competitive performance of the FPSO model in the quantity of MB removal from wastewater suggests that a complex adsorption phenomenon occurred involving van der Waals, hydrogen, and hydrophobic interactions between the MB and the chemical groups on Mn-MOF during the reaction. The rate constant k_f for the FPSO model showed that the rate of uptake of MB onto the surface of Mn-MOF was fast. The Webber-Morris intraparticle diffusion model was used to further process the data of the quantity of MB removed against time to determine the role and contribution of diffusion in the rate-controlling step of the adsorption process involving Mn-MOF. The size of the C values 0.16 mg/g obtained (Table 2) is insignificant and suggests that the chemical interactions on the Mn-MOF did not include surface phenomenon in the form of electrostatic interactions between the negatively charged adsorbent surface and the positively charged MB molecules [26].

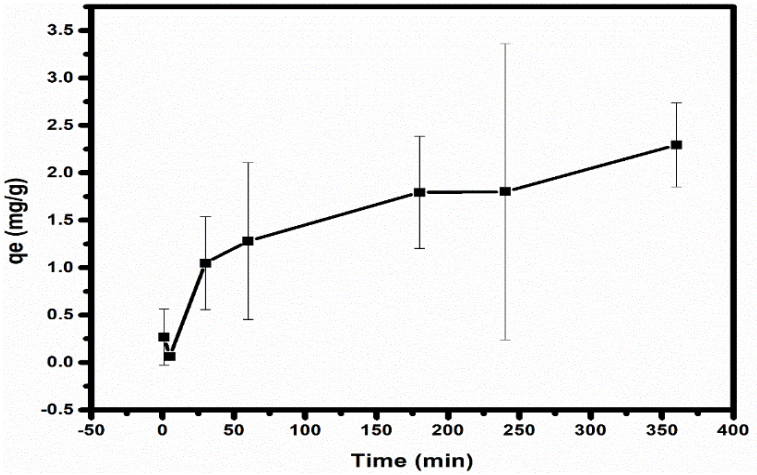


Fig. 4: Plot of Effect of Time on the Adsorption of MB onto Mn-MOF.

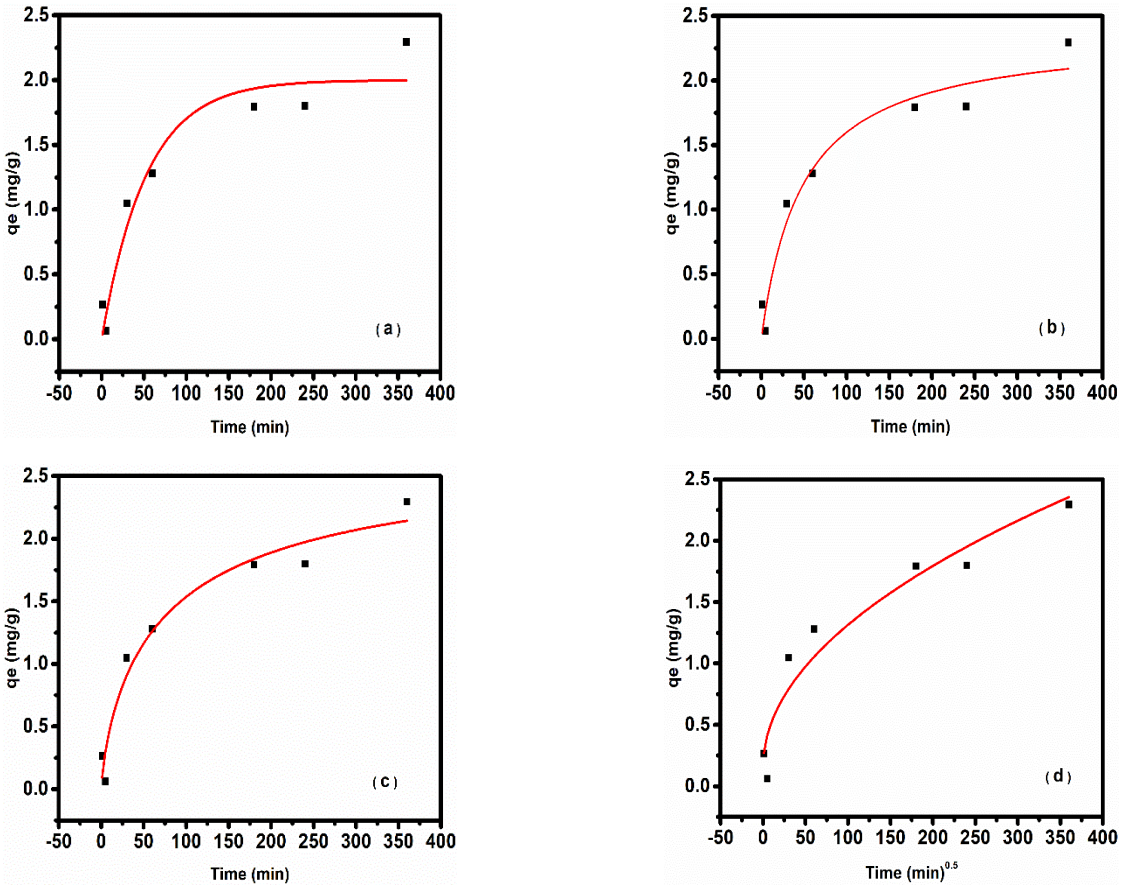


Fig. 5: Plots of (a) PFO, (b) PSO, (c) FPSO, and (d) Webber Morris IPD fits for the Description of the Adsorption Mechanism of MB onto Mn-MOF

Table 2: Kinetic Models Parameter for Adsorption of MB Onto Mn-MOF

Kinetic model	Parameter	Mn-MOF
Pseudo first order (PFO)	r^2	0.928
	q_e (mg/g)	2.00
	K	0.019
Pseudo-second order (PSO)	r^2	0.950
	q_e (mg/g)	2.37
	K	0.087
Fractal pseudo-second order (FPSO)	r^2	0.941
	K_f	0.012
	q_e (mg/g)	2.80
	A	0.772
Webber-Morris Intraparticle diffusion (IPD)	r^2	0.920
	K_{IPD}	0.115
	C (mg/g)	0.16
Experimental maximum adsorption	mg/g	1.30

Table 3: Adsorption Capacities of Selected Adsorbents Deployed in the Adsorptive Removal of Methylene Blue from Aqueous Media.

Adsorbent	Adsorbent capacity (mg/g)	Reference
MIL-101(Fe)-MOF	58.82	[27]
UiO-66-MOF	22.75	[28]
UiO-66-NO_2	41.7	[29]
MnO_2/IRMOF-3	11	[30]
Cu-MOF	169.2	[31]
Mn-MOF	2.80	This work

Table 3 shows the adsorption capacities demonstrated by MOF materials in previous works to this work. The Manganese-based composite (MnO2/IRMOF-3) possessed very low adsorption capacity compared to other MOFs in the table, but higher than Mn-MOF in this work, which was obtained from the time experiment where the kinetics were determined. However, it is expected that further work (on the effects of pH, concentration, and temperature; and on Mn-MOF-based composite) would optimize the adsorption capacity of Mn-MOF for MB.

4. Conclusion

The characterization of the Mn-MOF using FTIR spectroscopy showed the presence of Mn-O bonds, typical of the Metal-O bond in Mn-MOF. SEM analysis revealed a homogeneous laminar structure with closely stacked layers, while EDX confirmed the elemental composition of Mn-MOF, validating the synthesis of Mn-MOF. The adsorption studies followed the pseudo-second-order (PSO) kinetic model and, to a lesser extent, the fractal pseudo-second-order (FPSO) model in the removal of methylene blue (MB). This study concludes that Mn-MOF has significant potential for MB removal from aqueous solutions.

5. Recommendation

Further studies are undoubtedly necessary, particularly on the effects of pH, concentration, temperature, and Mn-MOF composite, to better understand the mechanism and thermodynamics governing the adsorption of MB by Mn-MOF to optimize the adsorption capacity. The effect of pH is envisaged to give a deeper understanding of the pHpzc characteristics of the pristine Mn-MOF and information on the optimum pH for maximum adsorption. The effect of concentration will also help in determining the optimum concentration for maximum adsorption, while the effect of temperature will also help to determine the optimum temperature for maximum adsorption. The study of a Mn-MOF-based composite provides insight into the kind of synergy required to improve the adsorption capacity for application. The effect of adsorbent dosage will also determine the optimum dose of adsorbent for maximum adsorption, while the adsorbent reusable experiment will determine whether the use of Mn-MOF will be economical if it is reusable at least 2-3 cycles. All these studies, if undertaken, will reveal the true potential of Mn-MOF for dye wastewater treatment and reuse. For lack of funds and research circumstances, this work could not address all these parameters.

Acknowledgement

The authors sincerely acknowledge the Department of Industrial Chemistry, Federal University Wukari, Taraba State, Nigeria, for providing laboratory access and academic resources necessary for conducting this study.

Conflict of Interest

The Authors have declared that no conflict of interest exists.

References

[1] Hussain S, Malik S, Cheema MJM, Ashraf MU, Waqas MS, Iqbal MM, Alia S, Anjum L, Aslam M, Afzal H. An overview on emerging water scarcity challenge in Pakistan, its consumption, causes, impacts, and remedial measures. *Big Data in Water Resources Engineering*. 2020;1(1):22–23. https://doi.org/10.26480/bdwre.01.2020.22.31.

[2] Mishra RK. Fresh water availability and its global challenge. *British Journal of Multidisciplinary and Advanced Studies*. 2023;4(3):1–78. https://doi.org/10.37745/bjmas.2022.0208.

[3] Khan WU, Ahmed S, Dhoble Y, Madhav S. A critical review of hazardous waste generation from textile industries and associated ecological impacts. *Journal of the Indian Chemical Society*. 2023;100(1):100829. https://doi.org/10.1016/j.jics.2022.100829.

[4] Akter T, Protity AT, Shaha M, Al Mamun M, Hashem A. The impact of textile dyes on the environment. In: Nanohybrid materials for treatment of textile dyes. Singapore: Springer Nature; 2023. p.401–431. https://doi.org/10.1007/978-981-99-3901-5_17.

[5] Hemashenpagam N, Selvajeyanthi S. Textile dyes and their effect on human beings. In: Nanohybrid materials for treatment of textile dyes. Singapore: Springer Nature; 2023. p.41–60. https://doi.org/10.1007/978-981-99-3901-5_3.

[6] Dutta P, Rabbi M, Sufian M, Mahjebin S. Effects of textile dyeing effluent on the environment and its treatment: A review. *Engineering and Applied Science Letters*. 2022;5:1–17. https://doi.org/10.30538/psrp-easl2022.0080.

[7] Alijanzadeh MB, Babayeemehr A, Rohani K, Mehrabani S, Aghajanpour F. Role of the World Health Organization in management of gastrointestinal diseases caused by contaminated water in children in the Middle East: A review. 2023.

[8] Alsukaibi AK. Various approaches for the detoxification of toxic dyes in wastewater. *Processes*. 2022;10(10):1968. https://doi.org/10.3390/pr10101968.

[9] Shindhal T, Rakholiya P, Varjani S, Pandey A, Ngo HH, Guo W, Taherzadeh MJ. A critical review on advances in the practices and perspectives for the treatment of dye industry wastewater. *Bioengineered*. 2021;12(1):70–87. https://doi.org/10.1080/21655979.2020.1863034.

[10] Sathya K, Nagarajan K, Carlin Geor Malar G, Rajalakshmi S, Raja Lakshmi P. A comprehensive review on comparison among effluent treatment methods and modern methods of treatment of industrial wastewater effluent from different sources. *Applied Water Science*. 2022;12(4):70. https://doi.org/10.1007/s13201-022-01594-7.

[11] AttahDaniel EB, Dikio ED, Nimibofa A, Wankasi D, Fanyana M, Diagboya PN. Adsorption investigation of a composite of metal-organic framework and polyethylene oxide hydrogel. In: *Nanomaterials, Nanoengineering and Nanosystems*. Springer; 2023. https://doi.org/10.1177/23977914231195748.

[12] Yu CX, Chen J, Zhang Y, Song WB, Li XQ, Chen FJ, Zhang YJ, Liu D, Liu LL. Highly efficient and selective removal of anionic dyes from aqueous solution by using a protonated metal-organic framework. *Journal of Alloys and Compounds*. 2021;853:157383. https://doi.org/10.1016/j.jallcom.2020.157383.

[13] Abdelghaffar R. Effluent dye removal by microwave-assisted activated carbon. 2023. https://doi.org/10.1007/978-3-031-41145-8.

[14] Kaur H, Devi N, Siwal SS, Alsanie WF, Thakur MK, Thakur VK. Metal–organic framework-based materials for wastewater treatment: superior adsorbent materials for the removal of hazardous pollutants. *ACS Omega*. 2023;8(10):9004–9030. https://doi.org/10.1021/acsomega.2c07719.

[15] Schoedel A. Secondary building units of MOFs. In: *Metal-organic frameworks for biomedical applications*. Woodhead Publishing; 2020. p.11–44. https://doi.org/10.1016/B978-0-12-816984-1.00003-2.

[16] Chakraborty G, Park IH, Medishetty R, Vittal JJ. Two-dimensional metal-organic framework materials: synthesis, structures, properties and applications. *Chemical Reviews*. 2021;121(7):3751–3891. https://doi.org/10.1021/acs.chemrev.0c01049.

[17] Zhao D, Song Q, Li Y, Li L, Yuan F, Yang Y, Zhang Z. Isoelectric substitution strategy to construct a partially charged MOF for C_2H_2 capture and selective dye adsorption. *ACS Applied Nano Materials*. 2023;6(11):9523–9530. https://doi.org/10.1021/acsanm.3c01191.

[18] Mantasha I, Saleh HA, Qasem KM, Shahid M, Mehtab M, Ahmad M. Efficient and selective adsorption and separation of methylene blue from mixture of dyes in aqueous environment employing a Cu(II)-based metal organic framework. *Inorganica Chimica Acta*. 2020;511:119787. https://doi.org/10.1016/j.ica.2020.119787.

[19] Ramesh M, Muthukrishnan M. Characterization of the metal-organic framework nanofibers prepared via electrospinning. In: *Electrospun Nanofibres*. CRC Press; 2023. p.1–33. https://doi.org/10.1201/9781003333814-1

[20] Nguyen VH, Nguyen TD, Van Nguyen T. Microwave-assisted solvothermal synthesis and photocatalytic activity of bismuth(III)-based metal–organic framework. *Topics in Catalysis*. 2020;63(11):1109–1120. https://doi.org/10.1007/s11244-020-01271-6.

[21] Ho YS, McKay G. Pseudo-second order model for sorption processes. *Process Biochemistry*. 1999;34(5):451–465. https://doi.org/10.1016/S0032-9592(98)00112-5

[22] Dikio ED, Farrah AM. Synthesis, characterization and comparative study of copper and zinc metal-organic frameworks. *Chemical Science Transactions*. 2013;2(3):1386–1394. https://doi.org/10.7598/cst2013.520.

[23] AttahDaniel EB, Dikio ED, Nimibofa A, Wankasi D, Fanyana M, Diagboya PN. Relative empirical evaluation of the aqueous sequestration of methylene blue using benzene-1,4-dicarboxylic acid linked lanthanum and zinc metal organic frameworks. *Water Air Soil Pollution*. 2022;233:442. https://doi.org/10.1007/s11270-022-05912-2.
[24] Cheng H, Li J, Meng T, Shu D. Advances in Mn-based MOFs and their derivatives for high-performance supercapacitor. *Small*. 2024;20(20):2308804. https://doi.org/10.1002/smll.202308804.
[25] Soltani A, Faramarzi M, Mousavi Parsa SA. A review on adsorbent parameters for removal of dye products from industrial wastewater. *Water Quality Research Journal*. 2021;56(4):181–193. https://doi.org/10.2166/wqrj.2021.023.
[26] Ebrahimi-Koodehi S, Ghodsi FE, Mazloom J. Ni/Mn metal–organic framework decorated bacterial cellulose and nickel foam as a visible-light photocatalyst and supercapacitive electrode. *Scientific Reports*. 2023;13(1):19260. https://doi.org/10.1038/s41598-023-46188-8.
[27] Eltaweila AS, Abd El-Monaem EM, Omer AM, Khalifa RE, Abd El-Latif MM, El-Subruiti GM. Efficient removal of toxic methylene blue dye from aqueous solution using MIL-101(Fe) metal-organic framework: isotherms, kinetics and thermodynamic studies. *Desalination and Water Treatment*. 2020;189:395–404. https://doi.org/10.5004/dwt.2020.25599.
[28] Al Amery N, Abid HR, Wang S, Liu S. Removal of methylene blue by bimetallic metal organic framework. *Journal of Applied Materials and Technology*. 2020;2(1):36–49. https://doi.org/10.31258/Jamt.2.1.36-49.
[29] Dinh HT, Tran NT, Trinh DX. Investigation into the adsorption of methylene blue and methyl orange by UiO-66-NO_2 nanoparticles. *Journal of Analytical Methods in Chemistry*. 2021;Article ID 5512174. https://doi.org/10.1155/2021/5512174.
[30] Geranmayeh S, Moradi A. A manganese oxide/MOF nanocomposite for the adsorption of methylene blue from aqueous solution. *Research Square*. 2022:9–20. https://doi.org/10.21203/rs.3.rs-1470334/v2.
[31] Wang S, Zhang L, Zhang M, Xu L, Hu Q, Yang T, Tu K, Wu M, Yu D. Enhanced methylene blue adsorption by Cu-BTC metal-organic frameworks with engineered particle size using surfactant modulators. *Water*. 2022;14:1864. https://doi.org/10.3390/w14121864.
[32] Al Amery N, Abid HR, Wang S, Liu S. Enhancing acidic dye adsorption by updated version of UiO-66. *Journal of Applied Materials and Technology*. 2020;1(2):54–62. https://doi.org/10.31258/Jamt.1.2.54-62.
[33] Liang Z, Liang Y, Yu P, Wang X. Ultrasonic-assisted in situ synthesis of MOF-199 on carboxylated cellulose fibers for efficient adsorption of methylene blue. *RSC Advances*, 2024, 14: 15095–15105. https://doi.org/10.1039/D4RA02099E
[34] Li H, Xu S, Du J, Tang J, Zhou Q. Cu@ Co-MOFs as a novel catalyst of peroxymonosulfate for the efficient removal of methylene blue. RSC advances. 2019;9(17):9410-20. https://doi.org/10.1039/C9RA01143A.
[35] Abbasi AR, Karimi M, Daasbjerg K. Efficient removal of crystal violet and methylene blue from wastewater by ultrasound nanoparticles Cu-MOF in comparison with mechanosynthesis method. Ultrasonics Sonochemistry. 2017 Jul 1;37:182-91. https://doi.org/10.1016/j.ultsonch.2017.01.007.